Electrocatalysis at Single Nanoparticles

Kleijn, S.E.F.

3

Electrochemical characterization of nano-sized gold electrodes fabricated by nano-lithography

Abstract

We report the lithographical fabrication of Au nanoelectrodes, with a geometrical surface area down to 160 nm $\times$ 1 µm. The geometrical surface area of the electrodes is verified using electron microscopy and by electrochemistry through the diffusion limited current of reversible redox couples. Moreover, the electrochemically active surface area of the electrodes is determined from the charges transferred in blank voltammetry. We believe these reproducible nanoelectrodes are well suited for use as probes in nano-electrochemistry research.

3.1 Introduction

Ultrasensitive electrochemical probes are made available through the fabrication of electrodes with nanosized dimensions. Their characteristics, such as fast mass-transport of reactants toward the electrode surface, sensitivity to extremely small currents and nanoscale dimensions have allowed the characterization of fast electron transfer reactions[1], single molecule detection[2] and individual enzyme immobilization.[3] In the field of electrocatalysis, ultrasmall amounts of platinum metal have been electrodeposited and studied as nanoelectrodes.[4, 5]

Several methods have been explored and used to fabricate such nano-sized electrodes. The currently most commonly used methods involve stretching a glass capillary containing a Pt wire of micrometer diameter, until a desired outer diameter is reached for the glass,[6–9] or etching a wire down to an ultrafine tip and coating all but the apex of the metal with an insulating polymer[10, 11] . Lithographical fabrication was introduced by preparing interdigitated arrays of electrodes[12, 13] and allows the design of individual nanoelectrodes patterned on top of a silicon oxide surface.[3, 14, 15] While the microelectrodes based on sealed wires are being produced with very small surface areas, there is no accurate, in-situ control over the actual electrode surface area during manufacture and it has to be determined after fabrication. Moreover, the success rate of such a delicate process is quite low[1, 6, 7, 16]. On the other hand, lithographically produced electrodes require fabrication expertise and electrochemical measurements on them have been troubled by parasitic capacitance.[3, 14, 15]

In this chapter we introduce a nanolithographic method for the reproducible fabrication of nanosized electrodes. Our aim is to demonstrate that these nano-electrodes can be fabricated reliably and reproducibly, and can be characterized by conventional electrochemical methods with low parasitic capacitance allowing measurement of both the real electrochemically active surface area and the geometric surface area of Au nanoelectrodes. To measure the electrochemically active surface area we use a technique commonly applied on macroscopic (single-crystal) electrodes, namely quantifying the charge transferred when stripping a monolayer of oxygen atoms from a Au surface in a blank voltammogram in acidic electrolyte[17]. Few blank voltammograms have been published of nanoelectrodes,[5, 8, 9, 11, 14–16] but they have not been used for accurate determination of the electrode surface area, presumably because they may be hard to generate reproducibly for such nano-sized electrodes. The electrochemically active surface area of the electrode measured can also be compared to geometric surface area as calculated from the diffusion limited current of reversible

redox couples,[18] and moreover, to the geometric surface area using electron microscopy. This leads to an electrochemical characterization of nano-sized electrodes to an extent that has not been achieved previously in the nano-electrochemistry literature.

3.2 Experimental

3.2.1 Chip Design

The design of the electrode assembly, schematically displayed in figure 3.1, has eight metal nanoelectrodes of 1 µm length and 1 µm, 500 nm, 250 nm and 100 nm width as the critical dimension. These electrodes are complimented with a microelectrode of 20 x 100 μm^2 that is used for calibration measurements. The electrodes are connected to leads that end as 1 x 1 mm^2 contact pads to connect to measurement apparatus. As a large part of the chip will be covered in (acidic) liquid electrolyte, the leads are covered by a thin film of silicon nitride that is chemically inert and non-conductive. The surface area of the electrodes that is exposed to the electrolyte is determined by the dimensions of a "window" opening the nitride film.

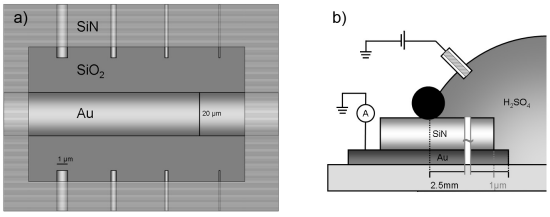

Figure 3.1: a) a top view schematic of the electrode assembly as designed, the microelectrodes are magnified 5× for visibility, a silicon nitride passivation layer ensures that only a designated part of the Au film is in contact with the aqueous phase. b) side view: Potential is applied between a reference electrode and the Au film at a contact pad, the current through the working electrode is measured using a low-noise current to voltage amplifier. The black circle represents the O-ring that contains the electrolyte. A scale bar indicates the average lead length covered by electrolyte.

3.2.2 Fabrication

Silicon wafers (4 inch diameter) with a 250 nm thermal SiO_2 layer were cleaned in fuming nitric acid, rinsed in water and dried with N_2. The wafers are coated with a bilayer of positive e-beam resists: PGMI (PolydiethylGlutarimide 7% in cyclopentanone, spun for 1 minute at 2500 RPM prebaked for 300 s at 200°C) and PMMA (poly-

methyl methacrylate 2% in anisole, spun for 1 minute at 6000 RPM, prebaked for 300 s at 175℃). After coating, the design for conductive leads and electrodes was patterned in the resist film using electron beam lithography. The subsequent two-stage resist development consisted of immersion in MIBK/IPA (Methyl isobutyl ketone / isopropanol; ratio 1:3 for 60 seconds) and iso-propanol (30s, to dilute the MIBK and stop development of the resist layers) for the PMMA top-layer, and in Microposit MF321 developer (10 seconds, followed by H_2O stopper for 15s) for the PGMI layer underneath. Onto the pattern, a film of Au (70nm thickness, 0.1 Å/s) on top of Ti (2nm, 0.5 Å/s) was deposited by means of electron beam evaporation, after which the resist was stripped off in hot Baker PRS3000 photoresist stripper (70℃). After lift-off, the wafer was cleaned in nitric acid, followed by oxygen plasma treatment to remove any residual resist. The wafer was subsequently coated with a passivation layer of 400nm SiN in a plasma-enhanced chemical vapor deposition (PCVD) chamber at 300℃. To pattern openings in the silicon nitride layer, in order to allow access of the electrolyte only to the electrode area and to open the contact pads for conductive contact, vinyl tape was applied to the area above the macroscopic contact pads before spincoating a layer of PMMA (950K, 8% in anisole, 1 minute at 1500 RPM) that was subsequently patterned using e-beam lithography and developed in MIBK/IPA (1:3, 120s) and IPA (30 s). Openings in the passivation layer could afterwards be made using dry etching in a fluor plasma(CHF_3 50 cm^3/min and O_2 2.5 cm^3/min, 50 W). All the nanofabrication preparations were carried out at the Van Leeuwenhoek cleanroom laboratory at the Delft University of Technology, additional fabrication details are provided in Appendix A.

3.2.3 Materials

Sulfuric acid (99.999%), ferrocenedimethanol (98%) and copper (II) sulfate pentahydrate (99.995%) were purchased from sigma-aldrich and used without further purification. Solutions were prepared using ultrapure water (18 M cm Milli-Q, Millipore.)

3.2.4 Electrochemistry

Cyclic Voltammograms were measured in a two-electrode setup, using a National Instruments analog-to-digital converter to both supply potential to the electrodes and read out the current that is amplified and converted by a Stanford SR570 low-noise current to voltage amplifier. To this end, labview software was prepared that averages the current measured in each potential step to further reduce the effect of interference

on the signal. The electrochemical chip was isolated in a home-built Faradaic cage, to which the electronic components were external. Inside the Faradaic cage, liquid electrolyte was supplied to the chip surface using a flow-cell setup that consists of a volume of electrolyte connected via Halar tubing to a polyether ether ketone (PEEK) nozzle with a viton O-ring surrounding its orifice that was firmly pressed onto the microchip. The PEEK nozzle outputs electrolyte to a drain vessel, and liquid flow is obtained by applying Ar overpressure in the electrolyte source volume.

3.2.5 Numerical Calculations

The rates of mass transfer towards the nanoelectrodes were derived numerically using finite element calculations in COMSOL multiphysics 4.2. The geometry consisted of a 100 µm x 20 µm box, on the bottom of which rest a nanoelectrode with length 11.3 µm, height 70nm and variable width ('swept' from 50 nm to 1150 nm in width in steps of 100 nm), and another cuboid (representing the SiN passivation layer) of width 100 µm, length 10 µm and height 400 nm, covering all except 1.3 µm of the box that represents the nanoelectrode. A mesh is generated that is finest near the electrode surface with the mesh cell size growing with distance from the 'electrode' surface. A solution is sought for the gradient in concentration of a diffusive species ('Ferrocenedimethanol'; D = $6.4 \times 10^{-6} cm^2/s$[19]) that has bulk concentration set to the values used in experiments described below (C = 0.4 mM). To this end the section of the surface of the electrode that is not blocked by the passivation layer has concentration of 0, corresponding to the steady state condition for an electrode performing a diffusion-limited outer-sphere electrochemical reaction, while the rest of the surfaces are set to bulk concentration. Disregarding effects of convection or migration, the value of the diffusive flux of reagent species towards the electrode yields the diffusion limited current directly when divided by the Faraday constant times the amount of electrons transferred (one for ferrocenemethanol).

3.3 Results

3.3.1 SEM

Figure 3.2a shows an electron micrograph of the area etched in the SiN insulation film to expose 8 nanoelectrodes and one microelectrode, the latter used for calibration purposes as well as counter/reference electrode. The thus exposed Au surface areas range from 0.2 to 1.3 μm^2, which is a slight increase over the designed area

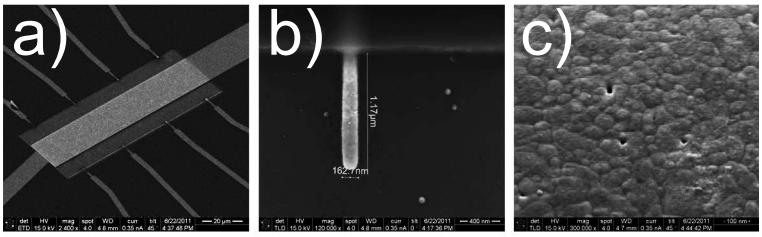

Figure 3.2: a: overview showing the Au nano electrodes of different sizes and the calibration electrode in the center. A rectangular window in the SiN passivation layer exposes the Au and SiO_2 below it to the aqueous electrolyte. b: Close up of a 100nm Au electrode, of which the voltammogram is displayed in figure 3.3b. c: Close up of Au surface roughness, visible with the sample at a 45 degree angle with respect to the electron beam.

as indicated in figure 3.2b. The electrodes patterned in the bi-layer resist are consistently 25nm wider on every side due to metal evaporated into the undercut profile. Moreover, the SiN window is almost 200 nm +/- 50 nm wider than expected, presumably caused by isotropic etching in the dry etch step. Zooming in (figure 3.2c), the electrodes appear slightly rough, consisting of 70 nm crystallites (estimated from SEM measurements) as expected for Au evaporated on a silicon wafer [20].

3.3.2 Blank Cyclic Voltammetry

The gold nano-electrodes shown in figure 3.2 were characterized electrochemically using cyclic voltammetry, the results of which are shown in figure 3.3. These measurements were made after a cleaning procedure that consisted of a 10 minute oxygen plasma treatment followed by boiling and rinsing the chip in milliQ water. Voltammograms shown are as measured directly after insertion and remain stable for at least 30 consecutive cycles. In figure 3.3a, the voltammogram measured at the calibration microelectrode shows features in its blank voltammogram which is comparable to the Au (111) surface.[21] In the positive going scan a series of peaks is observed from 1.3V, that is associated with the formation of a monolayer of oxygen atoms on the Au surface; in particular, the peak at 1.6 V is characteristic for Au(111) domains.[21] In the negative-going return scan, the oxide reduction peak shows a minimum at 1.15V followed by the double layer region. At potentials negative of 0V vs RHE, a reduction current corresponding to the hydrogen evolution reaction is observed.

Figure 3.3b shows the same voltammogram measured on one of the nanoelectro-

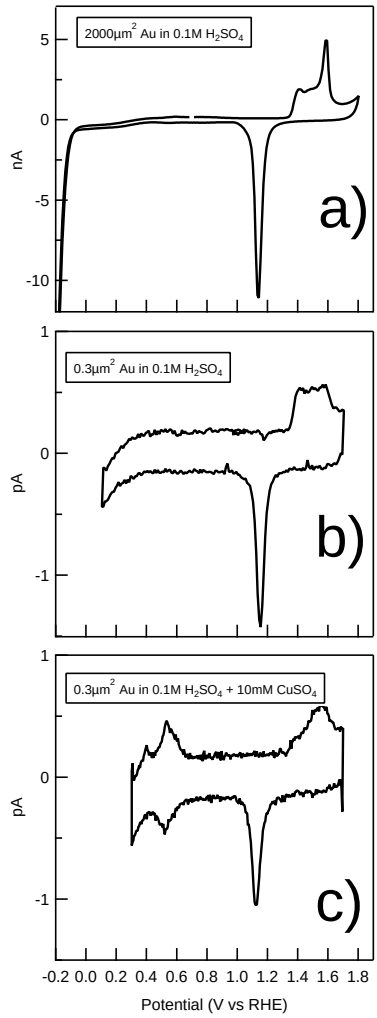

Figure 3.3: blank voltammograms of Au electrodes with designed areas of a) 2000 square micrometer and b) 0.2 square micrometer. Peaks typical for the surface oxide formation and stripping appear at the same potential values while the oxide stripping peak maximum scales four orders of magnitude. The underpotential deposition of Cu is displayed in c).

des with oxidation and reduction features at potentials identical to the calibration electrode. The main difference in the oxide-formation region is the absence of a strong peak at 1.6 V on the nanoelectrode, suggesting that these nanoelectrodes present fewer Au(111) terraces. Below 0.4V a reduction current is observed that we attribute to the reduction of oxygen gas that is permeating through the PEEK nozzle that

contains the electrolyte, followed by the hydrogen evolution current at potentials negative of 0 V. Another noticeable difference is the charging current in the double-layer region which is on average 140fA $\pm$22fA (corresponding to a capacitance of 2.8pF $\pm$0.5pF) and larger than expected when considering only the double layer contribution of the nano-electrode surface area, which has a tabulated value between 10 and 50 $\mu F/cm^2$,[18] or 0.1 - 0.5pF for a square micrometer. A larger capacitance is expected in the case of an electrode-on-silicon assembly, due to the charging interaction between the conductive electrolyte and the Au wiring, separated by the dielectric silicon nitride (as shown in figure 3.1). This contribution can be calculated using the equation for a model parallel plate capacitor:

$$C = \epsilon_r \epsilon_0 \frac{A}{d} \tag{3.1}$$

where ϵ_r is the relative permittivity of the dielectric material and ϵ_0 is the vacuum permittivity, A is the area of the smallest parallel plate and d is the separation of the two plates by the dielectric. Using the surface area of the Au wiring protected from liquid electrolyte (2.5mm x 4 µm) by the SiN dielectric ϵ_r = 7;[22]) of thickness 400nm yields 1.3pF for the microchip as designed. However, uncertainty in the determination of the area covered by the electrolyte, as well as in the actual thickness of the dielectric film affects the real value of the silicon nitride capacitance.

However, more significant is the capacitance between the Au film and the conductive silicon underneath the SiO_2 layer, which is calculated to amount to 30pF when the entire area of the Au film and the 500nm SiO_2 ϵ_r = 4;[23]) layer thickness is taken into account ($0.42\times10^{-6}m^2$ including the contact pads). Nevertheless, this source of parasitic capacitance can be removed by grounding the silicon in the substrate, allowing the capacitor to discharge into ground. The voltammogram in figure 3.3b is measured while grounding the silicon layer, and (considering the uncertainty in determining SiN capacitance) shows predominantly the SiN charging, with a minor contribution from the double layer charging.

3.3.3 Surface area determination

The real area of a metal surface equals the geometrical area defined by its boundaries only if it is an atomically flat plane, which is not the case for electrodes that are microscopically rough. The rougher a material is, the more surface area is exposed within the same geometrical enclosure. The ratio between the real, electrochemically active area of an electrode and its geometrical area is therefore called the roughness factor

of the electrode.

The electrochemically active surface area or the amount of surface atoms exposed to the electrolyte can be obtained from comparing the charge transferred when exactly one overlayer of gold oxide is reduced from the electrode (i.e. the integral of the cathodic current peak at 1.15V) to the value tabulated for this process on a flat gold surface, 400 $\mu C/cm^2$.[17] Dividing this electrochemically active surface area by the geometrical area measured using the SEM images gives the roughness factor for the nanoelectrode under consideration. For example, the voltammogram in figure 3.3b shows an oxidation and reduction wave in which 1.4pC $\pm$ 0.1pC is being transferred, yielding an electrochemically active surface area of 0.35 μm^2 $\pm$ 0.03 μm^2.

Attempts were also made to calculate the real surface area from the charge transferred when stripping a monolayer of underpotential deposited (UPD) copper off the electrode surface. A cyclic voltammogram describing this procedure is displayed in figure 3.3c, where the Cu UPD signal shows a reduction peak and a shoulder leading to the overpotential deposition. In the oxidative sweep two anodic peaks are observed, corresponding to the removal of a full Cu overlayer on the Au in two steps. The clear separation into two peaks is typical of a Cu UPD on Au(111) surfaces[24]. When the potential sweep is extended beyond the range displayed in fig. 3.3c, the overpotential deposition is observed as an exponential current decrease and, in the positive going return sweep, as a third oxidative peak. Nevertheless, the Cu UPD charges could not be evaluated reproducibly, because a parasitic current caused the voltammogram to slant, at different angles for different electrodes. Possibly the presence of Cu adatoms reduces the overpotential required to reduce dissolved oxygen, presence of which cannot be excluded in our current setup.

The average roughness factor obtained for the nanoelectrodes from the oxide stripping charge is 3.2 $\pm$ 0.2, while the charge transferred at the calibration electrode (figure 3.3a) corresponds to a roughness factor of 1.5. Previous electrochemical estimates of surface roughness on macroscopic evaporated Au thin-film electrodes range between 2 and 2.5[20, 25]. Since both the calibration electrode and the nanoelectrodes were deposited at the same time, it is not to be expected that their microstructure should change significantly. A previously published blank voltammogram measured on lithographically produced Au nanoelectrodes in the same potential domain,[14] however, exhibits an oxide stripping charge in excess of the geometric area by a factor close to 10, citing electrolyte leakage through the passivation layer as a possible cause for the unexpected surface area increase. Considering that nanoelectrodes have significantly more borderline with the passivating nitride layer per square micron compared

to the calibration electrode, it is to be expected that leakage plays a more important role for the nanoelectrodes. The presence of pinholes in the SiN, that may reveal additional surface area for the nanoelectrodes was tested by electrodepositing large quantities (i.e. 5 µm) of Cu. Analyses by optical microscopy afterwards showed no deposits along the unexposed Au leads.

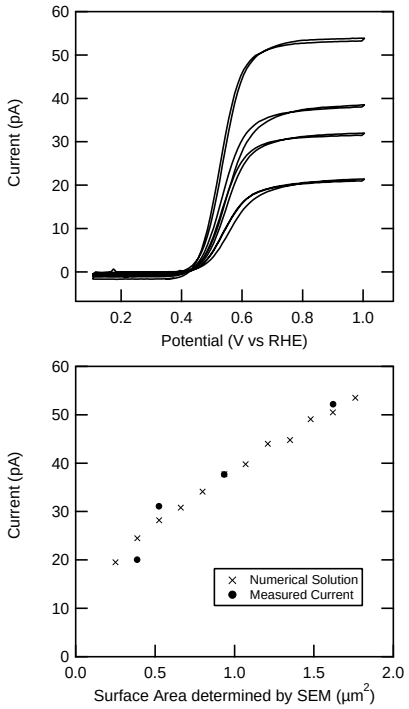

Figure 3.4: A) Cyclic voltammetry of Au nanoelectrodes in a solution containing 0.4mM ferrocenedimethanol and 0.1M sulfuric acid as a supporting electrolyte. B) shows the current plateau value versus the surface area as determined by SEM, for results of experiments and finite-element calculations.

In addition, the geometrical surface area of the electrodes was estimated by measuring the diffusion limited oxidation current of a redox couple with fast kinetics, which depends only on the concentration and the diffusion coefficient of the electroactive species and the electrode surface area. In figure 3.4a, the oxidation of ferrocenedimethanol (in 0.1M H_2SO_4 as supporting electrolyte) during a cyclic voltammogram is shown as a sigmoidal current wave. This CV-shape is expected for a diffusion-limited reaction at ultra-micro electrodes, with the plateau value a function of the electrode

geometrical surface area:[18]

$$I_{diff} = nFDCm_0A \tag{3.2}$$

Here n is the number of electrons transferred in the reaction, F is Faraday's constant, D is the diffusion coefficient of the redox molecule and C is its concentration in the bulk. The constant m_0 is related to the geometry of the electrode and its size; this constant can be provided analytically for shapes such as (hemi)spheres and disks. In the case of complicated shapes as used in this investigation, the value of m_0 can be found numerically.

To compare the measured currents to the values expected from theory, the diffusion-limited current equation was solved numerically, using a geometry model based on SEM measurements (the details of the calculations are explained in the experimental section). These calculated results are plotted in fig 3.4b together with the experimental findings.

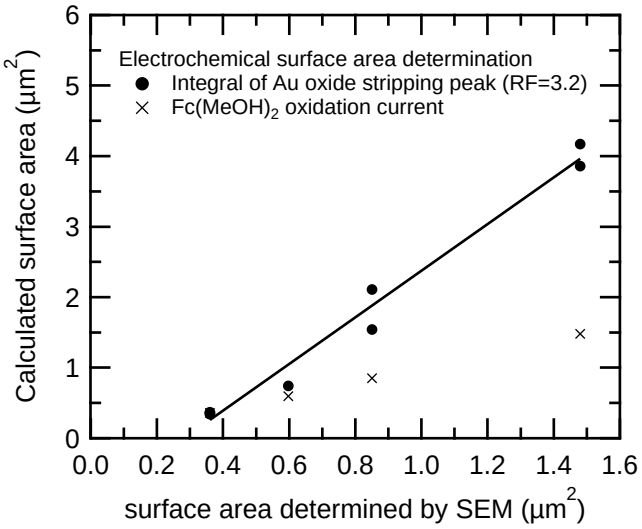

Figure 3.5: electrode surface areas calculated from the charge transferred during the stripping of an oxide monolayer (circles) and the diffusion limited current (crosses). A least squares fit reveals the roughness factor of the calculated area with respect to the geometrical area determined using the SEM.

In figure 3.4b, for the case of electrodes of 550nm and 1050nm in width, good agreement is found for the diffusion-limited current measured and the current derived from calculations, whereas the smaller electrodes show a deviation from the numerical

results of around 10-20%. Since the ferrocenedimethanol oxidation experiments are performed consecutively in the same solution, changes in the value of *C* and *D* are not expected. However, a deviation of 10-20% between the actual surface area and the value provided in the calculation for the smaller electrodes is reasonable once it is considered that fabrication errors such as overetching or lift-off errors have more impact on features of small area[3].

Both electrochemical methods used to determine the surface area of the electrodes are plotted against the surface area obtained from the electron microscopy in figure 3.5. The slopes differ since the measurements should theoretically supply the electrochemically active surface area (oxide monolayer stripping), and the geometrical surface area (diffusion limited current), respectively. The trends agree well with the designed surface area ratios of the electrodes and indicate a satisfactory control over the electrode surface area using this fabrication technique.

3.4 Conclusion

Using lithographic techniques, individually addressable gold electrodes were reproducibly fabricated with electrochemically active surface areas down to 0.3 μm^2. We succeeded in obtaining comparable calculated surface areas by measuring the oxide monolayer stripping integral and the diffusion limited ferrocenedimethanol oxidation current in comparison to the surface areas estimated from scanning electrode microscopy. These results demonstrate that we have developed a suitable and reliable technology for fabricating clean gold nanoelectrodes reproducibly. We will employ these electrodes in future nano-electrochemistry research.

Bibliography

[1] Penner, R. M.; Heben, M. J.; Longin, T. L.; Lewis, N. S. *Science* 1990, *250*(4984), 1118–1121.

[2] Zevenbergen, M. A. G.; Wolfrum, B. L.; Goluch, E. D.; Singh, P. S.; Lemay, S. G. *J. Am. Chem. Soc.* 2009, *131*(32), 11471–11477.

[3] Hoeben, F. J. M.; Meijer, F. S.; Dekker, C.; Albracht, S. P. J.; Heering, H. A.; Lemay, S. G. *ACS Nano* 2008, *2*(12), 2497–2504.

[4] Chen, S.; Kucernak, A. *J. Phys. Chem. B* 2004, *108*(37), 13984–13994.

[5] Chen, S.; Kucernak, A. *J. Phys. Chem. B* 2004, *108*(10), 3262–3276.

[6] Shao, Y.; Mirkin, M. V.; Fish, G.; Kokotov, S.; Palanker, D.; Lewis, A. *Anal. Chem.* 1997, *69*(8), 1627–1634.

[7] Pendley, B. D.; Abruña, H. D. *Anal. Chem.* 1990, *62*(7), 782–784.

[8] Jena, B. K.; Percival, S. J.; Zhang, B. *Anal. Chem.* 2010, *82*(15), 6737–6743.

[9] Guo, J.; Ho, C.-N.; Sun, P. *Electroanalysis* 2010, *23*(2), 481–486.

[10] Slevin, C. J.; Gray, N. J.; Macpherson, J. V.; Webb, M. A.; Unwin, P. R. *Electrochem. Commun.* 1999, *1*(7), 282–288.

[11] Mészáros, G.; Li, C.; Pobelov, I.; Wandlowski, T. . *Nanotechnology* 2007, *18*(42), 424004.

[12] Kittlesen, G. P.; White, H. S.; Wrighton, M. S. *J. Am. Chem. Soc.* 1984, *106*(24), 7389–7396.

[13] Bard, A. J.; Crayston, J. A.; Kittlesen, G. P.; Varco Shea, T.; Wrighton, M. S. *Anal. Chem.* 1986, *58*(11), 2321–2331.

[14] Mészáros, G.; Kronholz, S.; Karthäuser, S.; Mayer, D.; Wandlowski, T. *Appl. Phys. A: Mater. Sci. Process.* 2007, *87*(3), 569–575.

[15] Kronholz, S.; Karthäuser, S.; Mészáros, G.; Wandlowski, T.; van der Hart, A.; Waser, R. *Microelectron. Eng.* 2006, *83*(4-9), 1702–1705.

[16] Zuliani, C.; Walsh, D. A.; Keyes, T. E.; Forster, R. J. *Anal. Chem.* 2010, *82*(17), 7135–7140.

[17] Trasatti, S, O. P. *Pure Appl. Chem.* 1991, *63*(5), 711–734.

[18] Bard, A. J.; Faulkner, L. R. *Electrochemical Methods: fundamentals and applications;* Wiley, 2001.

[19] Zhang, W.; Gaberman, I.; Ciszkowska, M. *Electroanalysis* 2003, *15*(5-6), 409–413.

[20] Miyake, H.; Ye, S.; Osawa, M. *Electrochem. Commun.* 2002, *4*(12), 973–977.

[21] Angerstein-Kozlowska, H.; Conway, B. E.; Hamelin, A.; Stoicoviciu, L. *J. Electroanal. Chem. Interfac. Electrochem.* 1987, *228*(1-2), 429–453.

[22] Piccirillo, A.; Gobbi, A. L. *J. Electrochem. Soc.* 1990, *137*(12), 3910–3917.

[23] Gray, P. R.; Hurst, P. J.; Lewis, S. H.; Meyer, R. G. *Analysis and Design of Analog Integrated Circuits;* Wiley, 5 ed., 2009.

[24] Hachiya, T.; Honbo, H.; Itaya, K. *J. Electroanal. Chem. Interfac. Electrochem.* 1991, *315*(1-2), 275–291.

[25] Golan, Y.; Margulis, L.; Rubinstein, I. *Surf. Sci.* 1992, *264*(3), 312–326.